

# Comparative Analysis of Two Elastic Types of Surface-Crosslinked Gelatin Nanoparticles as Suitable Systems for Macromolecular Drug Delivery

Armin W. Novak, Stefan V. Pochmann, Alexander Horn, Agnes-Valencia Weiss, and Marc Schneider\*

With a steadily rising number of novel biopharmaceuticals in development, the demand for applicable delivery systems for macromolecular drugs persists. Polymeric nanoparticles, consisting of the natural product gelatin, present beneficial attributes for this application. To stabilize those nanoparticles without interfering with encapsulated macromolecules, surface-crosslinked gelatin particles are developed and thoroughly characterized for their physicochemical and mechanical properties. With only limited data available for the latter, investigating the elastic properties can offer a more comprehensive understanding of the crosslinking processes involved and of the gelatin particles' potential applications. In this study, protocols for surface-crosslinked gelatin particles type A (GNP-A) and B (GNP-B) are described. Significant differences between the two types of gelatin are reported regarding their physicochemical and mechanical properties. GNP-A consists of a lower crosslinking degree, leading to pronounced swelling in aqueous environments and softer nanoparticles. They possess contrary properties compared to the more extensively crosslinked and stiffer GNP-B. However, this doesn't affect encapsulation efficiency, allowing to develop nanoparticulate systems suitable for various applications by adjusting the particle properties while maintaining the same drug load. These findings provide a deeper understanding of polymeric gelatin particles and reveal the importance of investigating the mechanical properties of drug delivery systems during pharmaceutical development.

## 1. Introduction

Since the end of the twentieth century, therapeutic macromolecules, often referred to as biopharmaceuticals, are on a constant rise regarding new drug approvals by authorities. For the first time in history, the approval rate of these therapeutic macromolecules even overtook the one of small molecules in 2022, underlining the importance and the need of such medicines.<sup>[1]</sup> Although “macromolecule” not being a strictly defined term, this category, containing therapeutic peptides, antibodies, proteins, and nucleic acids, is in general described by its molecules' large size in the kilodalton range.<sup>[2–4]</sup> The field of biopharmaceuticals also possesses its own challenges when it comes to delivering these molecules to their respective target sites. Pharmaceutical hurdles such as instabilities, protein degradation, or lacking cell penetration need to be overcome by a suitable drug delivery system.<sup>[5]</sup> One currently applied technique is embedding or encapsulating of macromolecules into nanocarriers.<sup>[6,7]</sup> Nano-based drug delivery approaches can

A. W. Novak, S. V. Pochmann, A.-V. Weiss, M. Schneider  
 Department of Pharmacy  
 Biopharmaceutics and Pharmaceutical Technology  
 PharmaScienceHub (PSH)  
 Saarland University  
 66123 Saarbrücken, Germany  
 E-mail: [Marc.Schneider@mx.uni-saarland.de](mailto:Marc.Schneider@mx.uni-saarland.de)

A. Horn  
 Institute of Organic Chemistry  
 Saarland University  
 P.O. Box 151150, 66041 Saarbrücken, Germany

 The ORCID identification number(s) for the author(s) of this article can be found under <https://doi.org/10.1002/macp.202400513>

© 2025 The Author(s). Macromolecular Chemistry and Physics published by Wiley-VCH GmbH. This is an open access article under the terms of the [Creative Commons Attribution](https://creativecommons.org/licenses/by/4.0/) License, which permits use, distribution and reproduction in any medium, provided the original work is properly cited.

DOI: 10.1002/macp.202400513

provide a variety of advantageous properties, for instance controlling the release profile of the drug, shielding macromolecules from degradation and denaturation, or enhancing the cell and tissue penetration of the biological entities.<sup>[6,8–10]</sup> Throughout the broad field of nanocarrier systems, polymeric nanoparticles tend to play an increasingly important role in macromolecular drug delivery.<sup>[11]</sup> These particles can be divided into particles consisting of synthetic polymers and nanoparticles developed from natural polymers, within the biopolymer gelatin is intensively studied and shows promising characteristics as a drug delivery system for macromolecular drugs.<sup>[12–15]</sup>

The composition of the collagen-derived polymer gelatin is a blend of different polypeptide chains, consisting of distinct molecular weight fractions. Therefore, it is important to mention that the described properties for gelatin are commonly averaged for the whole protein throughout the different peptide chains.<sup>[16,17]</sup> Natural gelatin is obtained by hydrolysis of collagen and can be divided into two types, depending on the applied pre-treatment of the collagen. Type A gelatin is produced by acidic pre-treatment, resulting in an alkaline-acting gelatin, while type B is gained through alkaline pre-treatment of the collagen, yielding an acidic-acting polymer.<sup>[18]</sup> As a result of the pre-treatment process, gelatin types A and B consist of disparate physicochemical properties, originating from the alteration of their amino acid composition. While acidic treatment does not affect the amide groups of asparagine and glutamine amino acids, alkaline treatment impacts those groups by hydrolysis to carboxyl groups and triggers a conversion to aspartate and glutamate respectively.<sup>[19]</sup> This conversion of asparagine and glutamine to their acidic amino acid counterparts leads to two different isoelectric points (IEP) for gelatin type A and type B. Type A shows an IEP of 8–9 in contrast to type B with an IEP of 4.8–5.4.<sup>[20]</sup> Due to its unique properties, gelatin provides a suitable system for macromolecular drug delivery.<sup>[21–23]</sup> The proteogenic structure of gelatin, being on the one side beneficial for protein-based drug delivery, is accompanied by stability concerns on the other. Gelatin is unstable in aqueous environments and tends to dissolve under physiological conditions.<sup>[24]</sup> Therefore, gelatin particles have to be stabilized via crosslinking to create a suitable drug delivery system. For this purpose, a variety of different crosslinking methods were developed, including physical gelation by adjusting temperature or pH, enzymatic crosslinking, crosslinking using natural compounds such as genipin or plant-derived polyphenols, and chemical crosslinking.<sup>[24–27]</sup> Among the mentioned crosslinking options, chemical crosslinking using water-soluble compounds like formaldehyde or glutaraldehyde has been widely investigated in research.<sup>[28–30]</sup> Attributed to the compounds' high water solubility, crosslinkers are able to diffuse into the core of the gelatin particles and crosslink amino groups from two gelatin molecules, forming stable and water-insoluble networks. Regarding broad application for proteinaceous drugs, this unspecific reaction leads to covalent bonds between the gelatin network and the encapsulated drug, ensuing negative effects on the drug release and therefore its efficacy.<sup>[31,32]</sup> To overcome this obstacle, a novel approach on crosslinking the nanoparticles' surface using the water-insoluble crosslinker *N,N'*-diisopropylcarbodiimide (DIC) was established. DIC serves as a zero-length crosslinker, reacting with carboxyl groups of acidic amino acids by creating covalent bonds be-

tween these groups and primary amines. This crosslinker is widely used in peptide synthesis, forming peptide bonds between the reagents.<sup>[33]</sup> Due to its insolubility in water, the crosslinker cannot penetrate deeply into the particle, thus being unable to crosslink the encapsulated macromolecular drug. This method can be employed to produce stable, surface-crosslinked gelatin nanoparticles (GNP).<sup>[21]</sup> As a protein crosslinker, DIC possesses a toxicological potential derived from their ability to block ATP synthesis and oxidative phosphorylation.<sup>[34]</sup> Therefore, it's important to consider its biocompatibility after the surface-crosslinking of gelatin nanoparticles. As a zero-length crosslinker, DIC is not part of the formed peptide bonds and can be removed from the nanosuspension using suitable purification methods. DIC used for the crosslinking of gelatin nanoparticles can be considered to be biocompatible concluded from in vitro cytotoxicity tests performed after the purification of the final nanosuspension.<sup>[35]</sup>

During pharmaceutical development, nanoparticles are typically thoroughly characterized regarding certain physicochemical properties, that is, particle size, surface charge, or particle morphology. Despite the aforementioned parameters offer a good understanding of the interactions between nano-sized drug carriers and cells, further evaluation of additional particle attributes can provide beneficial insights.<sup>[36,37]</sup> With elastic properties being one of the lesser researched particle characteristics, the determination of these can open up new avenues in pharmaceutical exploration and aid in comprehending nanoparticle behavior.<sup>[38]</sup> Despite stiffer particles often showing an enhanced cellular uptake in vitro, this behavior is strongly dependent on the examined cell line and tissue type.<sup>[39–41]</sup> In contrast, other studies showed that softer particles are able to achieve a higher uptake in a variety of cancer cell lines when compared to their stiffer counterparts.<sup>[42–44]</sup> An additional study provided data on prolonged blood circulation time for softer nanoparticles in contrast to harder carriers, underlining the relevance of elastic properties in drug delivery.<sup>[45]</sup> This dissension in data regarding the various effects of mechanical particle properties highlights the need for further evaluations on this topic. Various methods exist for characterizing the mechanical properties of nanomaterials, including microfluidic approaches, quartz crystal microbalance methods, micro-rheology, and atomic force microscopy (AFM).<sup>[46]</sup> However, with AFM being currently the only method to determine the elasticity of single nanoparticles, it is the most accurate approach for the experiments conducted in this study. Atomic force microscopy evaluates particle elasticity by measuring the deflection of the cantilever on a sample surface. The resulting indentation of the cantilever tip into the nanoparticle can be plotted against the applied force. From these force curves, particle elasticities, calculated as Young's moduli, can be obtained.<sup>[47]</sup> Employing this principle, the mechanical properties of a variety of nanoparticles have been evaluated in the past, including gelatin nanoparticles.<sup>[30,48–50]</sup>

In this study, we focus on the thorough characterization of surface-crosslinked gelatin nanoparticles by investigation of established particle attributes as well as their mechanical properties. The utilization of gelatin as a natural polymer for macromolecular drug delivery was additionally evaluated using a macromolecular model drug. The hitherto applied method of nanoprecipitation for surface-crosslinked gelatin nanoparticles<sup>[51]</sup> was further refined, and an enhanced

**Table 1.** Physicochemical properties of gelatin nanoparticles type A and B crosslinked for 24–72 h. From left to right: gelatin type, crosslinking time (cl time), particle size measured as z-average, broadness of size distribution measured as polydispersity index (PDI),  $\zeta$ -potential, extent of particle crosslinking (cl extent), penetration depth of DIC (PD), entrapment efficiency of FITC-dextran (EE) and particle loading.  $N = 3$  individual experiments.

Gelatin type	cl time [h]	z-average [nm]	PDI	$\zeta$ -potential [mV]	cl extent [%]	PD [nm]	EE [%]	Loading [ $\mu\text{g mg}^{-1}$ ]
Type B	24	310.35 $\pm$ 6.95	0.139 $\pm$ 0.004	-32.42 $\pm$ 1.06	43.20 $\pm$ 3.20	26.6 $\pm$ 0.34	35.58 $\pm$ 6.49	16.99 $\pm$ 3.11
Type B	72	261.55 $\pm$ 12.85	0.175 $\pm$ 0.014	-30.07 $\pm$ 1.51	53.22 $\pm$ 4.19	29.3 $\pm$ 1.06	28.34 $\pm$ 3.89	13.49 $\pm$ 1.89
Type A	72	498.23 $\pm$ 33.12	0.164 $\pm$ 0.036	+4.82 $\pm$ 1.34	5.32 $\pm$ 1.23	4.50 $\pm$ 0.24	30.03 $\pm$ 1.79	14.82 $\pm$ 0.74

purification process was established. For the nanoparticles produced with this method, we were able to determine the degree of crosslinking and connect our findings with other properties of the two types of gelatin and the particles' mechanical attributes. For the first time, particle elasticity of surface-crosslinked gelatin nanoparticles was evaluated, revealing strong differences between the gelatin types A and B. Particles loaded with a macromolecule were also measured using AFM as a method for elasticity determination. The novel findings presented in this study offer a deeper understanding of gelatin as a drug carrier matrix material, as well as an enhanced method of producing such delivery systems. Additionally, the results underline the importance of the evaluation of mechanical properties for nanoparticles during pharmaceutical development and are therefore critical to help offset the data deficit in this particular area of research.<sup>[38]</sup>

## 2. Results

### 2.1. Physicochemical Properties and Drug Loading

Surface-crosslinked gelatin nanoparticles were evaluated regarding their physicochemical properties and their ability to efficiently encapsulate macromolecular drugs. **Table 1** provides an overview of the particle properties for GNPs consisting of type A or type B gelatin.

Particle size, measured as z-average, for GNP-B, decreases with prolonged crosslinking time. For type A particles a doubling in hydrodynamic diameter over type B particles could be observed when crosslinked under the same conditions for 72 h. Crosslinking for 24 h resulted in colloidal unstable particles for gelatin type A. The significant difference in size between type B and type A particles implies a less densely connected gelatin matrix, enabling the gelatin particles to swell to a higher extent as described later in the manuscript within the section "evaluation of particle swelling" in more detail. The polydispersity index of all three particle species was below 0.2 indicating a narrow particle size distribution.<sup>[52]</sup> The  $\zeta$ -potential of type B particles at pH 7 was  $\approx -31$  mV for both crosslinking times, showing that prolonged incubation time with DIC has no impact on the particles' charge. For gelatin type A particles, the  $\zeta$ -potential yielded a positive value of 4.82 mV, indicating the expected dependency of the  $\zeta$ -potential on the type of gelatin used for particle preparation. For a more in-depth analysis of the particles' charge, a pH-dependent titration of the  $\zeta$ -potential was performed. **Figure 1** illustrates the  $\zeta$ -potential for GNP-A and GNP-B in the pH range of 2 to 10.

At an acidic pH of 2, GNPs type A show a positive  $\zeta$ -potential of  $\approx 25$  mV, which subsequently decreases with a rising concentration of hydroxide ions in the medium, until reaching a neutral

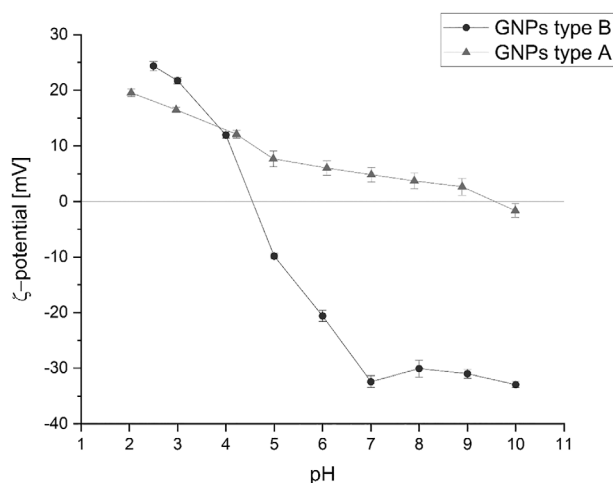


**Figure 1.**  $\zeta$ -potential of gelatin nanoparticles type A and B in the pH range of 2 to 10. For GNPs type A, a positive surface charge could be measured until eventually reaching the IEP at around pH 9.5. GNPs type B possess a positive  $\zeta$ -potential until pH 4.5, eventually changing to a negative charge after passing the IEP.  $N = 3$  individual experiments.

net charge at pH 9.5. After passing the isoelectric point (IEP), particles become negatively charged. For GNP type B, a more rapid decrease of the particles'  $\zeta$ -potential was observed. Starting at 20 mV at pH 2, a swift decline to the IEP at pH 4.5 was measured. Beyond the particles IEP, a negative  $\zeta$ -potential could be observed, eventually reaching a plateau phase at pH 7.

Regarding the crosslinking degree measured via 2,4,6-trinitrobenzenesulfonic acid (TNBS) assay, a prolonged incubation time with DIC from 24 to 72 h entailed an increase in crosslinking extent from 43.20% to 53.22% (Table 1). GNP-A expressed a significantly lower crosslinking extent (CE) of 5.32% compared to type B particles. Derived from the crosslinking degree, the penetration depth of DIC into the particle was calculated. Increasing the crosslinking time from 24 h of crosslinking to 72 h, a slight increase in penetration depth could be observed for type B particles. For type A particles crosslinked for 24 h, a determination of the penetration depth was not feasible due to the particles' colloidal instability. After crosslinking the particles for 72 h, the PD in gelatin type A particles is significantly lower compared to type B particles crosslinked over the same time span. For type A nanoparticles, DIC was able to crosslink only a thin layer according to the penetration depth of merely 4.5 nm into the particle.

Entrapment efficiency (EE) and drug loading of the particles were evaluated after particle digestion with trypsin. The EE of

**Table 2.** Poloxamer concentration in nanoparticle suspensions consisting of GNPs type A or B before and after the purification process with TFF. The suspensions before washing represent the positive control. After washing, the Poloxamer content was below the limit of quantification of 0.01 mg mL<sup>-1</sup>. *N* = 3 individual experiments.

Gelatin type	Poloxamer concentration in suspension [mg mL <sup>-1</sup> ]	
	Pre purification	Post purification
Type A	1.22 ± 0.26	<0.01
Type B	0.58 ± 0.06	<0.01

FITC-dextran with a molecular weight of 150 kDa showed no significant difference throughout all particle preparations. All nanoparticles showed an entrapment of 28–35% of the model drug. This finding indicates that crosslinking extent and gelatin type are not substantive for the encapsulation capability of macromolecular drugs into the prepared gelatin nanoparticles. Aligning with the entrapment efficiency, the drug loading of the particles ranged from 13.49 to 16.99 µg drug per mg nanoparticles absent of significant differences within the three distinct particle types. Furthermore, the entrapment efficiency for GNPs type A and B, crosslinked for 72 h respectively, was evaluated using a smaller-sized FITC-dextran with a molecular weight of 70 kDa. The results revealed a reduced EE for FITC-dextran 70 kDa of 6% for both particle types, compared to circa 31% for the larger 150 kDa molecule (Figure S2, Supporting Information). The calculated loading was reduced in the same manner to ≈3 µg mg<sup>-1</sup>.

## 2.2. Evaluation of the Purification Method

Poloxamer 188 is a triblock copolymer often used for colloidal stabilization of nanoparticles in research, as well as in already approved pharmaceutical products, positively effecting the particles' hydrodynamic diameter, size distribution and reducing agglomeration tendency.<sup>[53–55]</sup> During nanoprecipitation of the GNPs, poloxamer 188 was applied to the non-solvent phase acetone in a concentration of 2.25% (w/v). To remove the free stabilizer from the final suspension and maintain colloidal stable particles, tangential flow filtration was used as a purification method. The purification capability of the TFF was evaluated by performing a cobalt thiocyanate assay with a lower quantification limit of 0.01 mg mL<sup>-1</sup> for poloxamer 188. For all three nanoparticle species, the residual amount of stabilizer was below the limit of quantification and therefore not measurable after 2 h of purification. With the remaining amount of free poloxamer in the final suspension below 0.01 mg mL<sup>-1</sup>, it can be concluded that the stabilizer is successfully removed from the system. All samples were tested against a blank and a positive control, containing the unpurified suspension. Table 2 provides an overview of the poloxamer content of different nanosuspensions before and after washing via TFF.

For the positive control of GNP-B, a poloxamer concentration of 0.578 mg mL<sup>-1</sup> was observed, while for GNP-A the residual concentration of stabilizer was 1.217 mg mL<sup>-1</sup>. The difference in poloxamer concentration might be due to the smaller particle sizes in the formulation prepared from gelatin type B, resulting in a larger available surface area. Thus, this increased surface area

(≈70 times for 72 h-crosslinked particles; the area per poloxamer is approx. 12.8 nm<sup>2</sup><sup>[56]</sup> allowing to estimate the surface coverage) would lead to a higher amount of adsorbed poloxamer. In both cases, with a final residue of free poloxamer of under 0.001%, the TFF purification method was regarded as sufficient for the manufacturing procedure with respect to a potential application of the colloidal suspension.

For the detection of unreacted DIC residues in the final nanosuspension, gas chromatography (GC) was performed with the supernatant of the suspension after centrifugation. The respective chromatograms for type A and type B particles contained no peak for DIC when compared to the chromatogram with the crosslinker standard (see Figure S3, Supporting Information). The absence of DIC peaks in the tested nanosuspensions implies that the TFF purification method is suitable for the removal of unreacted DIC from the final nanosuspension.

## 2.3. Evaluation of the Effect of the Crosslinking Time

In order to develop monodisperse gelatin nanoparticles, different incubation times with DIC were investigated. Particles consisting of the two gelatin types A or B were crosslinked with 694 µL of DIC respectively and incubated for 24, 72 or 120 h. After crosslinking, the z-average and PDI of the purified particles were measured via dynamic light scattering. Figure 2 shows particle size and size distribution for GNP types A and B at different crosslinking times.

For gelatin type A particles, a clear dependency of particle size and size distribution on the incubation time with DIC was observed (Figure 2A). While 24 h of cl time provided insufficient stabilization for the nanoparticles, indicated by a z-average above 700 nm and a PDI of 0.33, accompanied by visible agglomeration, crosslinking for 72 h resulted in smaller, more monodisperse particles without agglomerates. Prolonging incubation time to 120 h showed no statistical superiority over 72 h of crosslinking. The significant reduction in particle size and PDI from 24 to 72 h of incubation was crucial for choosing the lead formulation for type A nanoparticles with a z-average of 498 nm and a PDI of 0.164.

GNP-B expressed no significant reduction in z-average with extending crosslinking time (Figure 2B). A DIC incubation of 24 h was sufficient for producing colloidal stable nanoparticles with desirable sizes of 310 nm and a PDI of 0.139. Derived from these results for gelatin type B particles shown in Figure 2B, 24 h crosslinked particles were chosen as the lead formulation while 72 h crosslinked particles, with a z-average of 262 nm and a polydispersity index of 0.175, were further evaluated to ensure comparability between type A and type B particles.

## 2.4. Evaluation of Particle Swelling

As significant differences between GNPs type A and type B were found during particle size evaluation, further experiments were conducted to identify the origin of these discrepancies. An obvious reason for a hydrogel material like gelatin might be the swelling behavior. Thus, this was investigated for the distinct particle species to check if the difference derives from particle preparation or is in connection to the lower crosslinking extent.



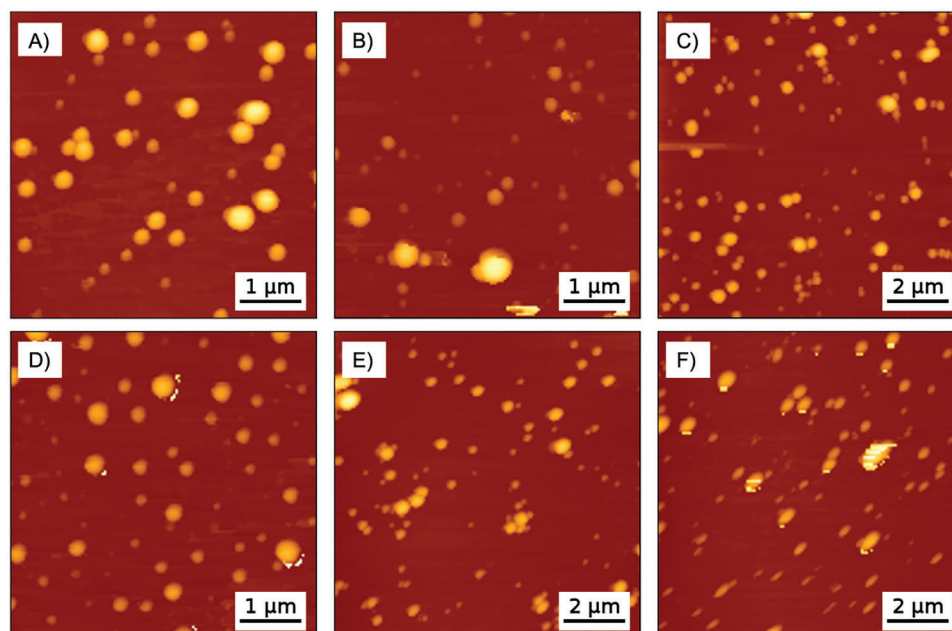


**Figure 4.** Selection of AFM images used for the calculation of Young's moduli for GNP-A unloaded (A) and loaded (D) crosslinked for 72 h, GNP-B crosslinked for 24 h unloaded (B) and loaded (E) and GNPs type B crosslinked for 72 h unloaded (C) and loaded (F). All samples were measured in water at 37 °C. For loaded particles, the model drug FITC-dextran 150 kDa was used.

Young's moduli of the distinct particles (**Figure 4**). For all samples, formulations showed single particles with no agglomerates formed during the production or purification process. GNP-A (4A) tend to show an increased particle diameter compared to GNP-B (4B, 4C). There was no visible difference between the unloaded particles (upper row) and the nanoparticles loaded with FITC-dextran 150 kDa (lower row). The overall particle size was for all samples in a range between 200–500 nm in diameter and corresponds to the sizes obtained by DLS.

The particle elasticity illustrated in **Figure 5** is calculated as Young's modulus for the three particle types, either as pure GNPs or loaded with FITC-dextran 150 kDa.

For nanoparticles consisting of gelatin type B, a clear dependency of particle stiffness on crosslinking time was visible. While blank particles crosslinked for 24 h possessed an average Young's modulus of 2716 kPa, those crosslinked for 72 h were significantly stiffer with Young's moduli of 3500 kPa. A similar trend could be observed for FITC-dextran loaded GNPs type B, where nanoparticles incubated for 72 h with DIC had a higher Young's modulus compared to particles with a shorter incubation time. The observed increase in particle stiffness could also be regarded as an implication for a higher crosslinking extent in these particles. For both type B GNPs, Young's moduli were significantly higher than for type A particles. Therefore, GNPs type A with Young's moduli of 249 kPa can be considered as comparatively soft particles. The pronounced difference in the mechanical properties of type B and type A particles also indicates a less densely crosslinked gelatin network for the latter.

The situation changed after the particles were loaded with a macromolecular model drug. For loaded particles produced with gelatin type B, a significant decrease of circa 500 kPa in particle stiffness could be observed. This decline was visible in 24 and

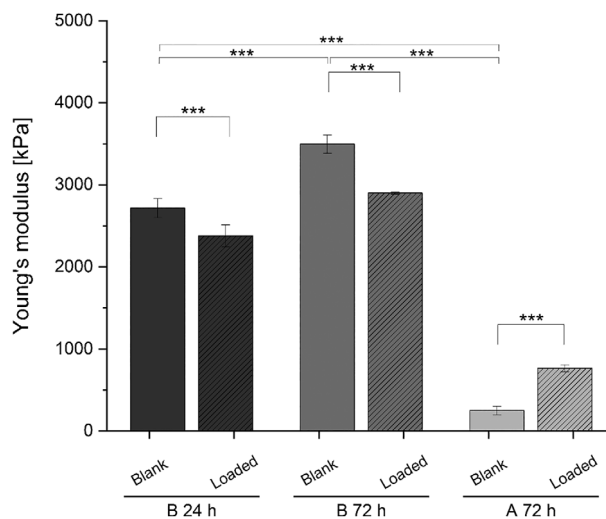


**Figure 5.** Elasticity of gelatin nanoparticles, depicted as Young's modulus, for blank and FITC-dextran 150 kDa loaded particles. Type A particles show significantly lower Young's moduli compared to type B particles and therefore are considered softer. While type B particles loaded with FITC-dextran are less stiff than blank particles, loaded type A GNPs are stiffer than their blank counterparts.  $N = 3$  individual experiments,  $*** = p < 0.001$ .

72 h crosslinked particles respectively. For type A GNPs, a contrary effect was discovered. Particles loaded with FITC-dextran showed an increase in particle stiffness from 249 to 765 kPa ( $\approx 3.1$ -fold increase). Nevertheless, when looking at the absolute values, loaded type A particles remained significantly softer than drug-loaded type B nanoparticles.

### 3. Discussion

#### 3.1. Physicochemical Properties and Drug Loading

Regarding the general physicochemical properties of surface-crosslinked gelatin nanoparticles, significant differences between the two types of gelatin A and B were observed when using identical production procedures (Table 1). For better comparability among type A and type B particles, type B nanoparticles were crosslinked for 72 h, although also 24 h would have provided stable particles. In contrast to this, type A particles did not show sufficient colloidal stability after 24 h. While the PDI for all particle species ranges below the value of 0.2, which is commonly regarded as a narrow particle size distribution,<sup>[57–59]</sup> the particles' hydrodynamic diameters show significant differences. The AFM images of the distinct particles validate the dynamic light scattering data by displaying a size range of the nanoparticles between 200 and 500 nm, with type A particles tending toward an increased particle diameter (Figure 4). Particles of the obtained sizes show significant uptake by macrophages in the literature.<sup>[60,61]</sup> Macrophages as potential targets are of increasing interest, for example, for interfering with chronic inflammations<sup>[62]</sup> or specific repolarization of macrophages for anti-tumor therapy.<sup>[63,64]</sup> Thus, these interactions can be important for future applications of surface-crosslinked GNPs, as internalization and decomposition of the particles by macrophages represent a possibility for the release of encapsulated drugs. Combining the low PDI of the produced nanoparticles with the ability for macrophage uptake, the developed systems is suitable for intended further parenteral applications. Further, no particle agglomeration could be observed during imaging, underlining the favorable PDI of below 0.2. As the amount of crosslinker DIC was kept constant during all experiments, changes in particle size can be explained both by incubation time (cl time) and the type of gelatin used.

For the incubation time, type B particles were crosslinked for 24 and 72 h respectively, with nanoparticles crosslinked for a longer time displaying only a slight decrease in z-average. This effect was also partly observed in previous studies.<sup>[21]</sup> Baseer et al. used DIC concentrations of 5 and 15 mg mL<sup>-1</sup>, where only the high crosslinker concentration had an impact on the particle size, resulting in smaller particles for prolonged incubation time. A lower DIC concentration of 5 mg mL<sup>-1</sup>, comparable to the 4.6 mg mL<sup>-1</sup> applied in this study, had no effect on the particles' z-average. Nevertheless, it is important to mention that temperature during crosslinking was kept constant in our experiments while it was varied in the aforementioned study.<sup>[21]</sup> The phenomenon of decreasing particle sizes with increasing crosslinking time has also been shown for gelatin nanoparticles crosslinked with glutaraldehyde, with particles crosslinked for 3 h consisting of smaller sizes compared to particles crosslinked for 0.5 h.<sup>[30]</sup> It was also observed, that with prolonged incubation time, the crosslinking extent for type B particles was raised by 10%. This increase implies that the crosslinking reaction between DIC and the amino acids in the gelatin matrix is not fully completed after 24 h of crosslinking. By becoming more densely interconnected from 24 to 72 h of incubation, the gelatin network tightens and is therefore not able to swell to the extent of shorter crosslinked particles in water, hence resulting in smaller

nanoparticles when immersed in an aqueous environment. The evaluation of particle swelling behavior is discussed further in the section "evaluation of particle swelling". The increased crosslinking extent is accompanied by a slightly deeper penetration depth of DIC into the particles, enlarging the crosslinked surface volume (Table 1). This observation aligns with the hypothesis of a more rigid and denser connected gelatin network with longer crosslinking time. This condensation of the network has also been observed for gelatin incubated with formaldehyde as a crosslinker.<sup>[65]</sup> The effect of a rising crosslinking extent with increasing crosslinking time has been described in the literature for the chemical crosslinkers glutaraldehyde and genipin as well.<sup>[30,66]</sup>

Apart from different incubation times, the type of gelatin used for particle preparation has a strong impact on the size of gelatin nanoparticles (Table 1). To explain this effect, a depiction of the crosslinking reaction between DIC and gelatin is crucial (Figure 6).

As shown in Figure 6, DIC reacts with carboxyl groups provided by the acidic amino acids glutamic acid and aspartic acid in the gelatin structure. Due to the alkaline pre-treatment of gelatin type B, further described in the introductory part, the amino acids glutamine and asparagine are converted to their acidic counterparts glutamic acid and aspartic acid. This process results in circa 65% more glutamic and aspartic acid in type B gelatin compared to type A gelatin.<sup>[67]</sup> The considerably lower presence of these acidic amino acids in gelatin type A leads to a significantly reduced crosslinking extent in this particle type (Table 1). A similar explanation has been given by Kuijpers et al. for gelatin crosslinked with 1-Ethyl-3-(3-dimethylaminopropyl)carbodiimide (EDC).<sup>[68]</sup> Potentially, the penetration depth of DIC is decreased as well, leaving the gelatin network mainly uncrosslinked except for a thin layer surrounding the particles' surface, calculated with a thickness of 4.5 nm. This offers an explanation for the nanoparticles' increased z-average, leaving the gelatin network in a state of less dense interconnection and therefore enabling a more pronounced swelling for the particles in aqueous environments. The low penetration depth of DIC into the particles is also a major advantage for macromolecular drug delivery, as less incorporated drug can be involved in the crosslinking process, enabling a higher delivery of therapeutically active drug to the target.

The differences in amino acid composition between type A and type B gelatin were also confirmed by  $\zeta$ -potential analysis of the two distinct particle types (Figure 1). Type A gelatin particles possess a surface charge of +4.82 mV at pH 7 compared to -30.07 mV for type B particles. These findings confirm an isoelectric point for gelatin type A in the basic pH range and for gelatin type B in the acidic milieu, derived from excess of acidic amino acids, which aligns with literature findings.<sup>[20]</sup>

Regarding the entrapment efficiency and loading of the macromolecular model drug FITC-dextran 150 kDa, no significant disparity between type A and type B particles was determined (Table 1). This is most likely linked to the fact that the preparation and particle formation are similar for the two approaches and thus involving the cargo in the same way. Crosslinking then happens after successful loading, providing particle stability and a diffusion barrier for the incorporated non-crosslinked

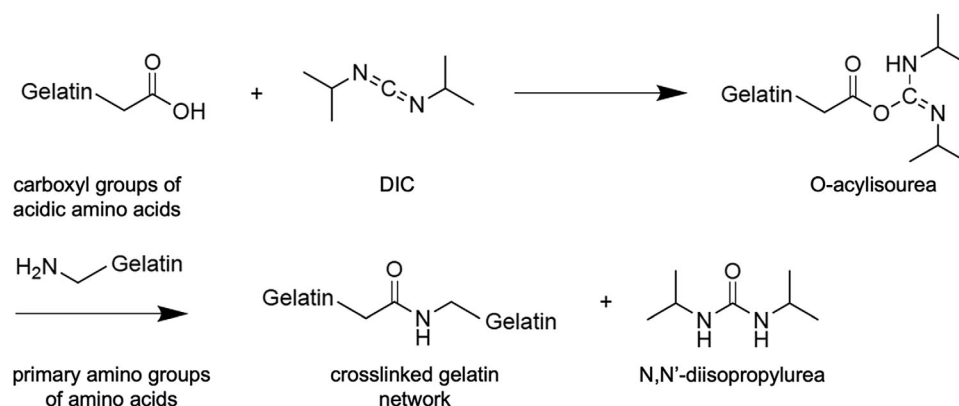


**Figure 6.** Overview of the crosslinking mechanism for DIC and gelatin. DIC reacts with carboxyl groups provided by acidic amino acids in the gelatin network. After the formation of O-acylisourea as an intermediate product, primary amino groups are linked to carboxyl groups, forming a peptide bond. As a zero-length crosslinker, DIC is not part of the final product, instead forming *N,N'*-diisopropylurea as a byproduct.

macromolecules. From this observation, we can conclude that the gelatin type has no impact on the particles ability to successfully entrap the model drug. With the considerably higher extent and DIC penetration depth of type B particles over type A particles, nanoparticles consisting of gelatin type A gain an advantage in macromolecular drug delivery, as less drug is prone to crosslinking from DIC. This finding is especially of interest as in literature mainly type B surface-crosslinked particles have been evaluated for macromolecular drug delivery.<sup>[21]</sup> Further, our results are in contrast to experiments carried out on glutaraldehyde core-crosslinked gelatin particles, in which a longer crosslinking time and therefore a higher crosslinking extent results in higher drug loading.<sup>[30,69]</sup> These contrary results underline the value of surface-crosslinked nanoparticles, as a constant drug loading could be achieved independent of the crosslinking extent. The average EE of  $\approx 31.3\%$  for all three particle types is in the same region as the entrapment in previous studies performed on surface-crosslinked GNPs.<sup>[35]</sup> As macromolecular drugs, such as monoclonal antibodies or therapeutic proteins, are generally substances with a strong target specificity and high in vivo efficacy, only low doses of these drugs need to be administered.<sup>[70]</sup> Derived from these specific advantages of biopharmaceuticals, the entrapment efficiency of the developed nanoparticles is sufficient for further applications as a drug delivery system.

The constant loading, independent of the gelatin type, was measured for the entrapment of FITC-dextran 70 kDa as well. While the overall entrapment efficiency and loading were reduced with the introduction of a smaller model drug, no differences between GNPs type A and type B could be observed (Figure S2, Supporting Information). A similar effect was observed in a study conducted on surface-crosslinked GNPs loaded with FITC-dextran of different molecular weights.<sup>[35]</sup> The lower EE and loading is likely due to the facilitated release of the smaller model drug through the pores in the gelatin network. The hindered diffusion of larger-sized molecules from a gelatin matrix was also described for glutaraldehyde crosslinked gelatin particles, pointing at a physical hinderance caused by the crosslinked network.<sup>[51]</sup>

### 3.2. Evaluation of the Purification Method

The gelatin nanoparticles developed in our study were purified from poloxamer 188 and unreacted DIC residues using tangential flow filtration. This method is widely used for the purification and concentration of nanoparticle suspensions and is considered to be an especially gentle method for these drug delivery systems.<sup>[71–73]</sup> While gelatin nanoparticles are often purified via centrifugation, this method proved to be inadequate for surface-crosslinked particles during the early development phase by leading to particle destruction and non-redispersible pellet formation.<sup>[74,75,51]</sup> Therefore, a previously described TFF method for surface-crosslinked gelatin particles was used and refined in terms of process efficiency by increasing the flow rate of the substrate.<sup>[35]</sup> Applying the enhanced method, it was possible to reduce filtration time from 8 to 2 h while maintaining the purification efficiency for the stabilizer and the unreacted crosslinker.

Tangential flow filtration is a suitable method for the removal of different stabilizers in nanosuspensions.<sup>[76]</sup> After a purification time of 2 h, all residues of free poloxamer were successfully removed from our nanosuspension (Table 2), leaving the samples with a stabilizer content of below  $0.01 \text{ mg mL}^{-1}$ , thus preventing the poloxamer to cause interferences during AFM imaging in subsequent experiments. Poloxamer 188 is an FDA-approved excipient for parental applications,<sup>[55]</sup> also commonly used in concentrations above  $0.01 \text{ mg mL}^{-1}$ .<sup>[77]</sup> On this basis, it can be concluded, that the reduction of free poloxamer below  $0.01 \text{ mg mL}^{-1}$  in our system is equivalent to a successful removal of the stabilizer from our final nanosuspension.

The dissimilarity between the initially used amount of stabilizer and the measured amount in the positive control can be caused by multiple dilution steps, including transfers of the suspension into different reaction vessels. As a stabilizer, poloxamer enriches at interfaces, such as liquid–solid-interfaces between nanosuspension and the walls of the reaction vessel, causing a loss of stabilizer with each transferring step.

The applied crosslinker DIC is generally regarded as a toxic compound, emphasizing the need of a thorough purification method.<sup>[78–80]</sup> After the TFF purification of our particles, no

unreacted DIC residues could be observed using gas chromatography (Figure S3, Supporting Information). The absence of a DIC peak in comparison to the DIC standard rates our purification method as suitable for the removal of crosslinker residues. With both undesirable residues successfully purged from the nanosuspension, the refined TFF method could be used in the development of surface-crosslinked gelatin nanoparticles.

### 3.3. Evaluation of the Effect of the Crosslinking Time

During the production of gelatin type B particles, a longer cl time has no significant impact on the particle size and PDI (Figure 2B). This aligns with the crosslinking extent after 24 h, being as high as 43.20% and therefore providing enough crosslinked functional side groups to obtain colloidally stable gelatin nanoparticles. Prolonging the incubation time above 24 h offers no advantages regarding the particle size and overall stability but resulted in higher Young's moduli. A different study also performed on DIC crosslinked gelatin type B particles, where particle size and PDI were monitored, concurs with these findings.<sup>[35]</sup> This plateau with no significantly beneficial changes to particle size and stability has also been described for other crosslinkers, such as glutaraldehyde or transglutaminase.<sup>[14,50,81]</sup>

For nanoparticles consisting of gelatin type A, a contrary behavior was observed (Figure 2A). While particles crosslinked for 24 h showed larger hydrodynamic diameters and high PDIs above 0.3, nanoparticles incubated for 72 and 120 h respectively displayed a more uniform size distribution and a decrease in particle size. Considering a crosslinking extent of 5.32% for 72 h crosslinked particles, it can be concluded that stable and monodisperse particle formation after 24 h for type A gelatin is not feasible due to an insufficient crosslinking of the gelatin network, leading to a polydisperse particle size distribution and visible agglomerates after the preparation process (Figure 2A). A continuation of DIC incubation after 72 h offers no additional benefits regarding particle stability, hence the 72 h crosslinked particles were chosen for all further experiments.

### 3.4. Evaluation of Particle Swelling

The swelling of the produced nanoparticles was evaluated to gain additional information on the effect of surface-crosslinking on the gelatin network. The swelling of gelatin as a hydrophilic polymer and its derived nanostructured drug carriers is well described in the literature for core-crosslinked systems.<sup>[82–84]</sup> However, there is a lack of data on the swelling behavior of surface-crosslinked gelatin particles. For this study, three different swelling scenarios were observed, representing the three stages in surface-crosslinked GNP production.

At first, the initial nanosuspension in acetone was evaluated, showing no differences in size between the three particle species (Figure 3, left). As a water-soluble polymer, gelatin is not prone to significant swelling in organic solvents.<sup>[85]</sup> These findings align with our hypothesis of surface-crosslinking, using a water-insoluble crosslinker to avoid the penetration of DIC deep into the hydrophilic particle core.

For particles suspended in water after the TFF process, clear differences between gelatin type A and type B particles are vis-

ible (Figure 3, middle). When in contact with aqueous environments, the porous gelatin network allows water to permeate into the particle.<sup>[82]</sup> Therefore, for a denser crosslinked network, less water can be absorbed and associated with the functional groups, resulting in a smaller particle size.<sup>[86,87]</sup> As gelatin type A particles possess a circa ten times lower crosslinking extent compared to type B particles, the overall less densely crosslinked network allows for higher water uptake. In addition, the system has more degrees of freedom to arrange in space. Both aspects lead to a pronounced particle swelling. Minor differences in swelling for type B particles crosslinked for 24 and 72 h can be explained with an equal mechanism but a higher restriction of the gelatine molecules in space.

The final drug delivery system was redispersed in water after lyophilization to form a nanosuspension (Figure 3, right). The effect on the completely dried particles was similar to the nanoparticles before freeze-drying, indicating that the gelatin network architecture is not affected by the drying process. Further, aggregation of nanoparticles after lyophilization is a known obstacle during particle formulation, often tackled by the addition of stabilizers or cryo- and lyoprotectants.<sup>[88,89]</sup> Displaying no increase in the intensity-weighted particle diameter, the developed surface-crosslinked nanoparticles are stable even in the absence of additional excipients. Additionally, the PDI of all three particle types after lyophilization is  $\approx 0.2$ , underlining the good redispersibility of the GNPs and the absence of larger agglomerates after freeze-drying. As interactions between these excipients and nanoparticulate formulations cannot be ruled out completely, the absence of additional compounds is clearly an advantage of the system.

### 3.5. Evaluation of Particle Elasticity

Looking at the observed size and swelling effects, the mechanical properties of the GNPs become of special interest. The mechanical properties of surface-crosslinked gelatin nanoparticles were measured using atomic force microscopy in the QI<sup>(TM)</sup> mode. Multiple images per sample were gathered for data assessment (Figure 4). Young's modulus was used as a parameter to determine nanoparticle elasticity, representing an established method to measure the elastic properties of particles.<sup>[90,91]</sup> For gelatin type B particles, a clear dependency on crosslinking time could be observed from AFM measurements (Figure 5, left and middle). The Young's moduli and therefore the particle elasticity increased with crosslinking duration. This effect can be explained by the higher crosslinking extent of nanoparticles incubated for 72 h compared to the 24 h particles. The increase in density of the gelatin network hinders the mobility of peptide chains. Furthermore, the crosslinking depth is increasing, thus leading to a stiffening of the nanoparticles. A similar effect was observed for gelatin nanoparticles crosslinked with glutaraldehyde.<sup>[30]</sup> Additionally, a correlation between the crosslinking extent and the particles' stiffness has been described for other nanoparticles in the same manner.<sup>[92]</sup> For the overall elasticity of the surface-crosslinked particles, it could be shown, that the developed particles possess much lower Young's moduli compared to core-crosslinked gelatin nanoparticles. While the particles crosslinked with the water-soluble compound glutaraldehyde displayed Young's moduli of  $\approx 14.26$  MPa when

crosslinked for 3 h, the surface-crosslinked particles had values of 2.7 MPa.<sup>[50]</sup> This data is perfectly in accordance with the crosslinking extent and the swelling behavior of the particles. With respect to potential applications, the demonstrated softness of surface-crosslinked gelatin particles can be beneficial.<sup>[93]</sup> For example, it was described in the literature that softer nanoparticles showed increased drug delivery potential to the target side and, dependent on the uptake pathway, the particle material, and cell type, an enhanced uptake in tumor cells, resulting in higher efficacy and a reduction in therapy accompanying adverse effects.<sup>[42,94–96]</sup>

Type B gelatin particles loaded with the macromolecular model drug FITC-dextran 150 kDa displayed significantly lower Young's moduli compared to their blank counterparts (Figure 5, left and middle). This effect could be observed in both, 24 and 72 h crosslinked particles. Weiss et al. described an analogous finding for core-crosslinked particles, also loaded with FITC-dextran.<sup>[30]</sup> As FITC-dextran possesses a carboxyl group itself, which can be crosslinked by DIC, a decrease in Young's modulus is rather unexpected. One possible explanation can be an intercalation of FITC-dextran molecules between the peptide chains in the gelatin network. This disturbance of the network can result in increased agility of the polymeric network and therefore lead to a softening of the particle. This would also be an explanation for the reduced Young's moduli in the aforementioned study by Weiss et al., as FITC-dextran cannot be crosslinked by glutaraldehyde due to a lack of free primary amino groups, while lysozyme, the alternatively loaded model drug, can be crosslinked by the aldehyde.<sup>[30]</sup> For lysozyme-loaded particles, there was no significant effect on the particles' elasticity measurable while for FITC-dextran-loaded nanoparticles, the interference of the gelatin network caused by the non-crosslinked macromolecule led to a softening of the particles. Another approach could be that the carboxyl group of FITC-dextran undergoes a steric hindrance from the large dextran appendix and the tricyclic xanthene structure, thus making it less accessible for DIC crosslinking. With these results taken into account, a disturbance of the gelatin network combined with a low affinity for crosslinking presents a plausible explanation for the decrease in Young's moduli for loaded gelatin particles compared to blank nanoparticles.

Regarding the mechanical properties of gelatin type A particles, a significant reduction in particle elasticity could be observed (Figure 5, right). This decrease in particle stiffness can be attributed to the less densely crosslinked gelatin network, resulting in a much lower crosslinking extent and penetration depth for DIC compared to type B particles. A relation between the density of the gelatin network and the alteration of mechanical properties has been described for gelatin type A, where a more densely crosslinked networked was accompanied by an increase in particle stiffness.<sup>[97]</sup> The decreased Young's modulus can additionally be attributed to the larger size and more pronounced swelling ability of the nanoparticles, as these result in higher overall agility of the gelatin chains in the network. The considerably softer type A particles can represent novel drug carriers for modified drug release, as previous studies had shown that softer particles showed a delayed uptake by macrophages and lung cells as well as prolonged blood circulation time.<sup>[45,50,61]</sup> This prolonged circulation time could open up new possibilities for the particles to be used for medium- or long-term drug delivery. A study carried out by

Merkel et al. showcased a clear dependency of circulation time on hydrogel particle elasticity, with softer particles possessing increasing elimination half-lives compared to stiffer particles.<sup>[98]</sup> Softer nanoparticles also displayed reduced splenic accumulation and therefore a prolonged blood circulation time *in vivo*.<sup>[45]</sup>

The FITC-dextran loading of gelatin type A nanoparticles showed contrary results to loaded type B particles (Figure 5, right). For the softer GNP-A, an increase in Young's modulus for loaded particles could be determined. Particle stiffening attributed to drug loading has been described for polymeric particles before, however, these particles were not crosslinked and a small molecule was used for drug encapsulation.<sup>[99]</sup> As gelatin type A possesses significantly fewer crosslinkable carboxyl groups compared to type B, the crosslinking reaction is considerably slower, also reflected in the evaluation of crosslinking time (Figure 2, right).<sup>[67]</sup> The additional presence of crosslinkable groups introduced by FITC-dextran, despite their reduced accessibility, might be impactful for this reaction. Regarding the low amount of carboxyl groups in type A gelatin, the reaction could proceed by crosslinking the unfavored groups of the model drug. This process is more likely to happen in type A gelatin, as type B gelatin can provide enough carboxyl groups for crosslinking by itself. Through this mechanism, an increase in Young's modulus for loaded type A particles is conceivable by the densening of the crosslinked gelatin network. Another explanation, which has not yet been evaluated, could be derived from charge-dependent effects from the loaded model drug. While GNP-B possesses a negative charge at pH 7, the  $\zeta$ -potential of type A nanoparticles is positive (Figure 1). FITC-dextran has a documented pKa value of  $\approx 5.9$ , leaving the majority of the model drug in a dissociated, negatively charged state at neutral pH.<sup>[100]</sup> For GNPs type A, attractive forces between the gelatin matrix and the FITC-dextran can be assumed, while for nanoparticles composed of gelatin type B repulsive forces between the model drug and the gelatin might appear. These repulsive forces could lead to a disturbance in the crosslinked matrix and therefore weaken the overall structure of the network, finally resulting in softer nanoparticles.

## 4. Conclusion

An approach for producing surface-crosslinked nanoparticles consisting of two distinctive types of gelatin using the hydrophobic crosslinker DIC was established. We were able to develop nanoparticles in a desirable size range of 250–500 nm with narrow size distributions. The macromolecular model drug FITC-dextran was successfully encapsulated in our particles, independent of the particles' size, crosslinking extent, and surface charge. Therefore, we accomplished the development of two distinct, yet equally suitable drug delivery systems for macromolecules, circumventing the negative effects from the crosslinker on the majority of the encapsulated drug. The entrapment efficiency of circa 31% of the system is suitable for the delivery of highly potent biopharmaceutical drugs. The different chemical compositions of the two types of gelatine resulted in different numbers of crosslinkable groups available. Thus, huge differences in crosslinking extent were obtained. In consequence, both surface-crosslinked types of GNPs display significantly different swelling behavior while conserving the colloidal characteristics. Originating from these differences, the mechanical properties of GNPs

type A and B differed from each other, leading to softer particles for gelatin type A. Both particle types showed severely decreased Young's moduli compared to core-crosslinked gelatin particles. The overall softness of the particles, as well as the variety between the two particle species, open new ways for their application in drug delivery. For stiffer type B particles, a faster uptake and therefore drug release at the target would be conceivable while for softer type A particles longer blood circulation time and slower uptake could be useful for long-acting drug administration in future studies. Loading of the particles showed different impacts in respect to the gelatin type, leading to a particle softening for type B particles and a stiffening in type A particles. In conclusion, the thorough characterization of surface-crosslinked GNPs, both physicochemically and mechanically, provides a deeper understanding of gelatin nanoparticles for macromolecular drug delivery and emphasizes the role of elastic particle properties during pharmaceutical development.

## 5. Experimental Section

**Nanoparticle Preparation:** Surface-crosslinked gelatin nanoparticles were produced using a refined nanoprecipitation method based on Baseer et al.<sup>[21]</sup> Depending on the preferred type of particles, gelatin type A (Bloom strength 90, Merck KGaA, Darmstadt, Germany) or type B (Bloom strength 75, Merck KGaA, Darmstadt, Germany) was dissolved in 1 mL Milli-Q water (Merck KGaA, Darmstadt, Germany) at 50 °C in a concentration of 20 mg mL<sup>-1</sup>. Gelatin solution (1 mL) was dispersed via syringe pump (Harvard Apparatus, Holliston, MA, USA) at 0.25 mL min<sup>-1</sup> in 15 mL of acetone containing 2.25% (w/v) Poloxamer 188 (Merck KGaA, Darmstadt, Germany) on a stirring plate (IKA-Werke GmbH and CO. KG, Staufen, Germany) at 750 rpm. After precipitation, particles were crosslinked using 694 µL DIC 69.17% (Merck KGaA, Darmstadt, Germany) in acetone. Crosslinking was conducted for 24 to 72 h at room temperature (RT) and constant stirring at 750 rpm. After incubation with DIC, 5 mL of the nanosuspension was transferred to 35 mL of Milli-Q water and stirred overnight at RT and 200 rpm for acetone evaporation.

**Nanoparticle Purification:** For purification, the aqueous nanosuspension was filtered through a 0.8 µm polycarbonate membrane (Whatman Nuclepore Track-Etched-Membrane, Merck KGaA, Darmstadt, Germany) and diluted with Milli-Q water to 300 mL. Subsequently, the suspension was purified via tangential flow filtration (TFF) using two Vivaflow 200 membranes (Sartorius AG, Göttingen, Germany) in serial connection for 2 h. After purification, the suspension was concentrated to 50 mL using the same TFF system. Purified surface-crosslinked GNPs were then freeze-dried (Alpha 3–4 LSCbasic, Martin Christ Gefriertrocknungsanlagen GmbH, Osterode am Harz, Germany) and stored at 4 °C until further use.

Fluorescein isothiocyanate dextran (FITC-dextran) loaded GNPs were produced by the addition of 1 mg FITC-dextran 150 kDa or 70 kDa (TdB Labs, Uppsala, Sweden) to the gelatin solution before nanoprecipitation. Nanoparticles were then manufactured and purified according to the unloaded particles.

**Purification Method Evaluation—Evaluation of Poloxamer 188 Residues:** Poloxamer 188 residues were evaluated by a colorimetric assay based on the formation of cobalt thiocyanate complexes with poloxamer.<sup>[101]</sup> In brief, 5 mg of freeze-dried GNPs were redispersed in 10 mL Milli-Q water and centrifuged at 20 000 × g for 20 min. Two milliliters of supernatant, 2 mL of ethyl acetate (Merck KGaA, Darmstadt, Germany) and 1 mL of cobalt thiocyanate solution (obtained by dissolving 20 g ammonium thiocyanate and 3 g cobalt (II) nitrate (both Merck KGaA, Darmstadt, Germany) in 100 mL Milli-Q water) were mixed and centrifuged at 1000 × g for 5 min. The upper two layers composed of water and ethyl acetate were discarded and the pellet was redispersed with 2 mL ethyl acetate. The process was repeated until the upper layer was colorless. Subsequently, the pellet was dissolved in 10 mL of acetone and the absorbance was mea-

sured against a blank at λ = 624 nm using a plate reader (Tecan infinite M200, Tecan Trading AG, Männedorf, Switzerland). Poloxamer 188 content was calculated based on calibration data with a limit of quantification of 0.1 mg mL<sup>-1</sup>. A positive control, containing GNPs before TFF purification, was treated likewise for type A and type B particles.

**Purification Method Evaluation—Evaluation of DIC Residues:** The presence of unreacted DIC residues was evaluated using gas chromatography (GC).<sup>[21]</sup> Five milligrams of lyophilized GNPs were dispersed in 5 mL dichloromethane (Merck KGaA, Darmstadt, Germany) and centrifuged at 20 000 × g for 20 min. The supernatant was withdrawn and analyzed using a gas chromatograph equipped with a flame ionization detector (Shimadzu GC-2010, Kyoto, Japan). A DIC solution, containing 2 mg mL<sup>-1</sup> DIC in dichloromethane, was prepared as a standard.

**Nanoparticle Characterization—Particle Size and ζ-Potential:** The size and polydispersity index (PDI) of the nanoparticles were measured using the z-average obtained via dynamic light scattering (Zetasizer Ultra, Malvern Panalytical, Malvern, UK). Samples were diluted tenfold with Milli-Q water before measurement.

ζ-potential was evaluated using a pH titration method, ranging from pH 2 to pH 10. Sample preparation was performed by dispersing 5 mL of the nanosuspension in 10 mL Milli-Q water and adjusting the pH to 2 with 0.5 M HCl. Titration was then carried out using an autotitrator (MPT-2, Malvern Panalytical, Malvern, UK) in combination with the Zetasizer Ultra. ζ-potential was measured via electrophoretic light scattering.

For the analysis of particle swelling behavior, sizes were determined either in acetone, representing the unswollen state, or Milli-Q water at pH 7 demonstrating the swollen state of the particles. For each experiment, the particles were diluted tenfold with the respective dispersant. All experiments were conducted as a technical and experimental triplicate.

**Nanoparticle Characterization—Crosslinking Extent and Penetration Depth:** The crosslinking extent (CE) of the GNPs obtained through DIC crosslinking was evaluated using a 2,4,6-trinitrobenzenesulfonic acid (TNBS) assay to determine uncrosslinked ε-amino groups.<sup>[20]</sup> For analysis, 5 mg lyophilized, crosslinked GNPs were dispersed in 1 mL 4% sodium bicarbonate solution followed by the addition of 1 mL 0.5% TNBS solution (both Merck KGaA, Darmstadt, Germany). For complete reaction, the suspension was heated to 40 °C for 4 h. After the incubation time, 3 mL of 6 N HCl were added before hydrolyzing the gelatin for 1 h (120 °C, 1.03–1.17 bar). After dilution to 10 mL with Milli-Q water, 5 mL ethyl acetate was added to extract unreacted TNBS. The procedure was repeated until complete colorlessness of the organic phase was observed. Subsequently, a 5 mL aliquot was withdrawn, and absorbance was measured at λ = 349 nm via plate reader against a blank. As a reference, uncrosslinked gelatin particles were prepared and measured in an according manner. The crosslinking extent was then calculated according to a method described by Khan et al.<sup>[51]</sup>

Penetration depth (PD) of the crosslinker into the gelatin matrix was approximated using Equation (1).

$$CE = \frac{r_p^3 - (r_p - PD)^3}{r_p^3} \quad (1)$$

with CE representing the crosslinking extent in percent,  $r_p$  the particle radius, and PD the penetration depth. The equation was valid assuming that the authors have a full and homogeneous crosslinking which was then transferred to the dimension of the particle assuming the crosslinking density to be unchanged. A more detailed derivation of Equation (1) can be found in Figure S1 (Supporting Information).

**Nanoparticle Characterization—Entrapment Efficiency and Loading:** To determine the encapsulation of FITC-dextran 150 and 70 kDa in the GNPs, the fluorescence intensity of loaded FITC-dextran was evaluated after particle digestion.<sup>[51]</sup> Briefly, 2 mg of lyophilized GNPs were suspended in 5 mL phosphate-buffered saline (PBS) at RT. After the addition of 0.5 mg trypsin (AppliChem GmbH, Darmstadt, Germany) per mg gelatin, the particles were digested at 37 °C for 6 h. The obtained solution was filtered through 0.22 µm polyethersulfone membranes before measuring fluorescence emission intensity at λ = 520 nm with an excitation wavelength of

$\lambda_{\text{ex}} = 485 \text{ nm}$ . The entrapment efficiency (EE) was calculated using Equation (2).

$$EE = \frac{\text{Mass of FITC} - \text{dextran measured (mg)}}{\text{Mass of FITC} - \text{dextran used (mg)}} \times 100 \quad (2)$$

The loading of the GNPs was evaluated by use of the following Equation (3).

$$\text{Loading} = \frac{\text{Mass of FITC} - \text{dextran measured (\mu g)}}{\text{Mass of GNPs (mg)}} \quad (3)$$

**Nanoparticle Characterization—Particle Elasticity:** The elastic properties of gelatin nanoparticles were evaluated using AFM. Sample preparation and measurement were based on a method by Weiss et al.<sup>[30]</sup> In brief, silica wafers (Plano GmbH, Wetzlar, Germany) were sonicated for 5 min in an ultrasonic bath (Elmasonic B, Elma Schmidbauer GmbH, Singen, Germany) in high-purity ethanol (Merck KGaA, Darmstadt, Germany) to remove any contaminating residues. After purification, wafers were dried under nitrogen gas. For GNP-B, wafers were incubated with an aqueous 1% branched polyethyleneimine (bPEI) 25 kDa solution (Merck KGaA, Darmstadt, Germany) for 15 min in order to gain positively charged coated wafers. Excess bPEI was removed with Milli-Q water and silica wafers were left for drying. Subsequently, one drop of sample suspension was placed on the wafer and incubated for 1 min. Following incubation, the wafer was rinsed with Milli-Q water and stored in liquid until the measurement was performed.

For GNP-A, one droplet of nanosuspension was placed on the uncoated wafer surface and incubated for 10 min. Afterward, the excess sample was removed with Milli-Q water and likewise stored in liquid until AFM measurements were conducted on the same day.

AFM images were obtained using a JPK NanoWizard 3 AFM (JPK Instruments, Berlin, Germany) with samples measured in an aqueous environment at 37 °C. For force spectroscopy, the AFM was equipped with a MLCT cantilever (Bruker France Nano Surfaces, Wissembourg, France) using the tip D of the cantilever with a spring constant of 0.03 N m<sup>-1</sup> and a nominal resonance frequency of 15 kHz. Spring constant and sensitivity were calibrated prior to the measurements by the thermal noise method<sup>[102]</sup> on a blank silica wafer. For data acquisition, the AFM was used in a quantitative imaging mode (QI<sup>(TM)</sup>-mode), setting the image dimensions to 5 × 5 μm or 10 × 10 μm with a final resolution of 128 × 128 pixels. Pixel dwell time was set to 50 ms with 700 μm z-height while a loading force of 1 nN was applied.

The obtained AFM images with underlying force data were processed with the JPK SPM Data Processing software (version 6.1.172, JPK Instruments, Berlin, Germany). For each particle, four pixels, taken from the particle center, were evaluated extracting the underlying force–distance curves. For calculation of the Young's moduli, each force curve was treated with a series of data processing measures.<sup>[30]</sup> Concisely, the spring constant and sensitivity of the cantilever obtained by calibration were applied to set the cantilever deflection. For vertical offset correction, the baseline was subtracted and the contact point between the tip and the sample surface was defined. Subsequently, a tip-sample separation was performed before the force curves were fitted using an alteration from the Hertz model for quadratic pyramidal probes.<sup>[103]</sup> The Young's moduli of all four force-distance curves per particle were averaged, resulting in 30 values per sample in total.

**Data Evaluation and Statistics:** All data was evaluated using OriginPro 2021b software (version 9.8.5.212, OriginLab Corporation, Northampton, MA, USA). For statistical analysis between two data sets a two-sample *t*-test was performed. Multiple data sets were evaluated by using one-way ANOVA with a Bonferroni post hoc test. All original data presented in this paper was obtained by an experimental triplicate.

## Supporting Information

Supporting Information is available from the Wiley Online Library or from the author.

## Acknowledgements

The authors would like to thank Prof. C. Wagner and Prof. F. Lautenschläger for the possibility to use the JPK NanoWizard 3 AFM. Philipp Sonntag is thanked for the kind provision of the ChemDraw software.

Open access funding enabled and organized by Projekt DEAL.

## Conflict of Interest

The authors declare no conflict of interest.

## Author Contributions

A.N. dealt with conceptualization, formal analysis, investigation, methodology, project administration, validation, visualization writing the original draft, and writing the review and editing. SVP dealt with the investigation and methodology. A.H. dealt with the investigation. A.V.W. dealt with the conceptualization, project administration, supervision, and writing the review and editing. M.S. dealt with the conceptualization, project administration, supervision, and writing the review and editing.

## Data availability statement

QI-data for AFM evaluations as well as size and  $\zeta$ -potential data presented in this work is available under the following link:<https://cloud.hiz-saarland.de/s/EFCWt3PZHNDNwzBK>.

## Keywords

atomic force microscopy, crosslinking, elasticity, hydrogel nanoparticles, macromolecular drug delivery, mechanical nanoparticle properties, nanogel

Received: December 17, 2024  
Revised: February 11, 2025  
Published online: February 20, 2025

- [1] M. Senior, *Nat. Biotechnol.* **2023**, *41*, 174.
- [2] H. He, W. Dong, J. Gong, J. Wang, V. C. Yang, *Front. Chem. Eng. China* **2010**, *4*, 10.
- [3] G. Walsh, E. Walsh, *Nat. Biotechnol.* **2022**, *40*, 1722.
- [4] J. Yang, J. Kopeček, *J. Controlled Release* **2014**, *190*, 288.
- [5] R. Juliano, *Biochem. Soc. Trans.* **2007**, *35*, 41.
- [6] V. Agrahari, V. Agrahari, A. K. Mitra, *Ther. Delivery* **2016**, *7*, 257.
- [7] G. Tosi, J. T. Duskey, J. Kreuter, *Expert Opin. Drug Delivery* **2020**, *17*, 23.
- [8] L. L. Tundisi, J. A. Ataíde, J. S. R. Costa, D. D. F. Coêlho, R. B. Liszbinski, A. M. Lopes, L. Oliveira-Nascimento, M. B. De Jesus, A. F. Jozala, C. Ehrhardt, P. G. Mazzola, *Colloids Surf., B* **2023**, *222*, 113043.
- [9] D. Peer, J. M. Karp, S. Hong, O. C. Farokhzad, R. Margalit, R. Langer, *Nat. Nanotechnol.* **2007**, *2*, 751.
- [10] L. Zhang, F. Gu, J. Chan, A. Wang, R. Langer, O. Farokhzad, *Clin. Pharmacol. Ther.* **2008**, *83*, 761.

- [11] M. A. Beach, U. Nayanathara, Y. Gao, C. Zhang, Y. Xiong, Y. Wang, G. K. Such, *Chem. Rev.* **2024**, *124*, 5505.
- [12] C. J. Coester, K. Langer, H. Von Briesen, J. Kreuter, *J. Microencapsulation* **2000**, *17*, 187.
- [13] A. Kakkar, G. Traverso, O. C. Farokhzad, R. Weissleder, R. Langer, *Nat. Rev. Chem.* **2017**, *1*, 0063.
- [14] K. Ofokansi, G. Winter, G. Fricker, C. Coester, *Eur. J. Pharm. Biopharm.* **2010**, *76*, 1.
- [15] N. Sahoo, R. K. Sahoo, N. Biswas, A. Guha, K. Kuotsu, *Int. J. Biol. Macromol.* **2015**, *81*, 317.
- [16] I. J. Haug, K. I. Draget, in *Handbook of Hydrocolloids*, (Eds.: G. O. Phillips, P. A. Williams), Vol. 2, Elsevier B.V, Amsterdam, Netherlands **2009**, Ch. 6.
- [17] D. Liu, M. Nikoo, G. Boran, P. Zhou, J. M. Regenstein, *Annu. Rev. Food Sci. Technol.* **2015**, *6*, 527.
- [18] J. Alipal, N. A. S. Mohd Pu'ad, T. C. Lee, N. H. M. Nayan, N. Sahari, H. Basri, M. I. Idris, H. Z. Abdullah, *Mater. Today: Proc.* **2021**, *42*, 240.
- [19] K. Su, C. Wang, *Biotechnol. Lett.* **2015**, *37*, 2139.
- [20] W. A. Bubnis, C. M. Ofner, *Anal. Biochem.* **1992**, *207*, 129.
- [21] A. Baseer, A. Koenneke, J. Zapp, S. A. Khan, M. Schneider, *Macromol. Chem. Phys.* **2019**, *220*, 1900260.
- [22] A. O. Elzoghby, *J. Controlled Release* **2013**, *172*, 1075.
- [23] O. Madkhali, G. Mekhail, S. D. Wettig, *Int. J. Pharm.* **2019**, *554*, 224.
- [24] A. B. Bello, D. Kim, D. Kim, H. Park, S.-H. Lee, *Tissue Eng., Part B* **2020**, *26*, 164.
- [25] N.-C. Cheng, B. T. Estes, T.-H. Young, F. Guilak, *Tissue Eng., Part A* **2013**, *19*, 484.
- [26] A. Hayashi, S.-C. Oh, *Agric. Biol. Chem.* **1983**, *47*, 1711.
- [27] G. Strauss, S. M. Gibson, *Food Hydrocolloids* **2004**, *18*, 81.
- [28] M. Azami, M. Rabiee, F. Moztarzadeh, *Polym. Compos.* **2010**, *31*, 2112.
- [29] G. Mugnaini, R. Gelli, L. Mori, M. Bonini, *ACS Appl. Polym. Mater.* **2023**, *5*, 9192.
- [30] A.-V. Weiss, D. Schorr, J. K. Metz, M. Yildirim, S. A. Khan, M. Schneider, *Beilstein J. Nanotechnol.* **2022**, *13*, 778.
- [31] K. A. Janes, P. Calvo, M. J. Alonso, *Adv. Drug Delivery Rev.* **2001**, *47*, 83.
- [32] E. Leo, M. Angela Vandelli, R. Cameroni, F. Forni, *Int. J. Pharm.* **1997**, *155*, 75.
- [33] A. El-Faham, F. Albericio, *Chem. Rev.* **2011**, *111*, 6557.
- [34] F. J. Ruder, W. Guyer, J. A. Benson, H. Kayser, *Pestic. Biochem. Physiol.* **1991**, *41*, 207.
- [35] A. Baseer, *Ph.D. Thesis*, Universität des Saarlandes, (Saarbrücken) **2019**.
- [36] N. D. Donahue, H. Acar, S. Wilhelm, *Adv. Drug Delivery Rev.* **2019**, *143*, 68.
- [37] Z. Zhao, A. Ukidve, V. Krishnan, S. Mitragotri, *Adv. Drug Delivery Rev.* **2019**, *143*, 3.
- [38] A.-V. Weiss, M. Schneider, *Beilstein J. Nanotechnol.* **2023**, *14*, 1149.
- [39] A. C. Anselmo, M. Zhang, S. Kumar, D. R. Vogus, S. Menegatti, M. E. Helgeson, S. Mitragotri, *ACS Nano* **2015**, *9*, 3169.
- [40] C. Huang, P. J. Butler, S. Tong, H. S. Muddana, G. Bao, S. Zhang, *Nano Lett.* **2013**, *13*, 1611.
- [41] C. Yao, O. U. Akakuru, S. G. Stanciu, N. Hampp, Y. Jin, J. Zheng, G. Chen, F. Yang, A. Wu, *J. Mater. Chem. B* **2020**, *8*, 2381.
- [42] P. Guo, D. Liu, K. Subramanyam, B. Wang, J. Yang, J. Huang, D. T. Auguste, M. A. Moses, *Nat. Commun.* **2018**, *9*, 130.
- [43] H. Tang, H. Ye, H. Zhang, Y. Zheng, *Soft Matter* **2015**, *11*, 8674.
- [44] J. Tao, W. Shi, K. Chen, W. Lu, A. J. Elbourne, L. Bao, L. Weng, X. Zheng, X. Su, Z. Teng, L. Wang, *Biomater. Sci.* **2023**, *11*, 822.
- [45] L. Zhang, Z. Cao, Y. Li, J.-R. Ella-Menye, T. Bai, S. Jiang, *ACS Nano* **2012**, *6*, 6681.
- [46] M. Li, Z. Gao, J. Cui, *Langmuir* **2022**, *38*, 6780.
- [47] A. Vinckier, G. Semenza, *FEBS Lett.* **1998**, *430*, 12.
- [48] J. Choi, L. Bastatas, E. Lee, K. T. Mutiso, S. Park, *J. Ind. Eng. Chem.* **2022**, *113*, 283.
- [49] H. Li, Y. Han, T. Duan, K. Leifer, *Appl. Phys. Lett.* **2019**, *115*, 053104.
- [50] A.-V. Weiss, T. Fischer, J. Iturri, R. Benitez, J. L. Toca-Herrera, M. Schneider, *Colloids Surf., B* **2019**, *175*, 713.
- [51] S. A. Khan, M. Schneider, *Macromol. Biosci.* **2013**, *13*, 455.
- [52] M. Danaei, M. Dehghankhold, S. Ataei, F. Hasanzadeh Davarani, R. Javanmard, A. Dokhani, S. Khorasani, M. R. Mozafari, *Pharmaceutics* **2018**, *10*, 57.
- [53] D. Jain, R. Athawale, A. Bajaj, S. Shrikhande, P. N. Goel, R. P. Gude, *Colloids Surf., B* **2013**, *109*, 59.
- [54] F. Yan, C. Zhang, Y. Zheng, L. Mei, L. Tang, C. Song, H. Sun, L. Huang, *Nanomedicine: NBM* **2010**, *6*, 170.
- [55] W. N. Chen, M. F. Shaikh, S. Bhuvanendran, A. Date, M. T. Ansari, A. K. Radhakrishnan, I. Othman, *Curr. Neuropharmacol.* **2022**, *20*, 799.
- [56] A. M. Hillery, A. T. Florence, *Int. J. Pharm.* **1996**, *132*, 123.
- [57] H. Hoseini, M. R. Jaafari, A. Golabpour, A. A. Momtazi-Borojeni, M. Karimi, S. Eslami, *Sci. Rep.* **2023**, *13*, 18012.
- [58] V. B. Patravale, A. A. Date, R. M. Kulkarni, *J. Pharm. Pharmacol.* **2010**, *56*, 827.
- [59] L. Wu, J. Zhang, W. Watanabe, *Adv. Drug Delivery Rev.* **2011**, *63*, 456.
- [60] L. Leclerc, W. Rima, D. Boudard, J. Pourchez, V. Forest, V. Bin, P. Mowat, P. Perriat, O. Tillement, P. Grosseau, D. Bernache-Assollant, M. Cottier, *Inhalation Toxicol.* **2012**, *24*, 580.
- [61] M. Yildirim, A.-V. Weiss, M. Schneider, *Pharmaceutics* **2023**, *15*, 199.
- [62] N. G. Sukubo, P. Bigini, A. Morelli, *Beilstein J. Nanotechnol.* **2025**, *16*, 97.
- [63] S. Al-Fityan, B. Diesel, T. Fischer, E. Ampofo, A. Schomisch, V. Mashayekhi, M. Schneider, A. K. Kiemer, *Pharmaceutics* **2023**, *15*, 1895.
- [64] F. J. Van Dalen, M. H. M. E. Van Stevendaal, F. L. Fennemann, M. Verdoes, O. Iliina, *Molecules* **2018**, *24*, 9.
- [65] P. Dalev, E. Vassileva, J. E. Mark, S. Fakirov, *Biotechnol. Tech.* **1998**, *12*, 889.
- [66] A. Bigi, G. Cojazzi, S. Panzavolta, N. Roveri, K. Rubini, *Biomaterials* **2002**, *23*, 4827.
- [67] T. Baydin, O. A. Aarstad, M. J. Dille, M. N. Hattrem, K. I. Draget, *Food Hydrocolloids* **2022**, *127*, 107535.
- [68] A. J. Kuijpers, G. H. M. Engbers, J. Krijgsveld, S. A. J. Zaat, J. Dankert, J. Feijen, *J. Biomater. Sci. Polym. Ed.* **2000**, *11*, 225.
- [69] A. Bahoor, R. Ahmadi, M. Heydari, M. Bagheri, A. Behnamghader, *Inorg. Chem. Commun.* **2023**, *154*, 110856.
- [70] S. Mitragotri, P. A. Burke, R. Langer, *Nat. Rev. Drug Discovery* **2014**, *13*, 655.
- [71] G. Dalwadi, H. A. E. Benson, Y. Chen, *Pharm. Res.* **2005**, *22*, 2152.
- [72] H.-W. Liu, Y. Hu, Y. Ren, H. Nam, J. L. Santos, S. Ng, L. Gong, M. Brummet, C. A. Carrington, C. G. Ullman, M. G. Pomper, I. Minn, H.-Q. Mao, *ACS Appl. Mater. Interfaces* **2021**, *13*, 30326.
- [73] T. Musumeci, A. Leonardi, A. Bonaccorso, R. Pignatello, G. Puglisi, *PNT* **2018**, *6*, 48.
- [74] S. Balthasar, K. Michaelis, N. Dinauer, H. Von Briesen, J. Kreuter, K. Langer, *Biomaterials* **2005**, *26*, 2723.
- [75] Y.-C. Chen, S.-H. Yu, G.-J. Tsai, D.-W. Tang, F.-L. Mi, Y.-P. Peng, *J. Agric. Food Chem.* **2010**, *58*, 6728.
- [76] G. Dalwadi, V. B. Sunderland, *Drug Dev. Ind. Pharm.* **2007**, *33*, 1030.
- [77] P. Adams-Graves, A. Kedar, M. Koshy, M. Steinberg, R. Veith, D. Ward, R. Crawford, S. Edwards, J. Bustrack, M. Emanuele, *Blood* **1997**, *90*, 2041.
- [78] M. Matsumoto, H. Ito, A. Tateishi, Y. Kobayashi, K. Satoh, K. Numata, H. Miyakawa, *J. Appl. Toxicol.* **2023**, *43*, 1840.
- [79] I. Surh, M. Behl, S. A. Elmore, R. S. Chhabra, *Cutaneous Ocul. Toxicol.* **2012**, *31*, 177.

- [80] Y. Utku, A. Rohatgi, B. Yoo, K. Kirshenbaum, R. N. Zuckermann, N. L. Pohl, *J. Chem. Educ.* **2010**, *87*, 637.
- [81] S. Fuchs, M. Kutscher, T. Hertel, G. Winter, M. Pietzsch, C. Coester, *J. Microencapsulation* **2010**, *27*, 747.
- [82] A. K. Bajpai, J. Choubey, *J. Mater. Sci.: Mater. Med.* **2006**, *17*, 345.
- [83] H. Khan, R. N. Shukla, A. K. Bajpai, *Mater. Sci. Eng., C* **2016**, *61*, 457.
- [84] C. M. Ofner, H. Schott, *J. Pharm. Sci.* **1986**, *75*, 790.
- [85] S. Boral, A. N. Gupta, H. B. Bohidar, *Int. J. Biol. Macromol.* **2006**, *39*, 240.
- [86] A. J. Kuijpers, G. H. M. Engbers, P. B. Van Wachem, J. Krijgsveld, S. A. J. Zaat, J. Dankert, J. Feijen, *J. Controlled Release* **1998**, *53*, 235.
- [87] S. Moshayedi, H. Sarpoolaky, A. Khavandi, *Polym. Eng. Sci.* **2021**, *61*, 3094.
- [88] W. Abdelwahed, G. Degobert, S. Stainmesse, H. Fessi, *Adv. Drug Delivery Rev.* **2006**, *58*, 1688.
- [89] P. Fonte, S. Reis, B. Sarmiento, *J. Controlled Release* **2016**, *225*, 75.
- [90] D. Guo, G. Xie, J. Luo, *J. Phys. D: Appl. Phys.* **2014**, *47*, 013001.
- [91] S. N. Raja, A. C. K. Olson, A. Limaye, K. Thorkelsson, A. Luong, L. Lin, R. O. Ritchie, T. Xu, A. P. Alivisatos, *Proc. Natl. Acad. Sci. USA* **2015**, *112*, 6533.
- [92] A. C. Anselmo, S. Mitragotri, *Adv. Drug Delivery Rev.* **2017**, *108*, 51.
- [93] X. Banquy, F. Suarez, A. Argaw, J.-M. Rabanel, P. Grutter, J.-F. Bouchard, P. Hildgen, S. Giasson, *Soft Matter* **2009**, *5*, 3984.
- [94] P. Gurnani, C. Sanchez-Cano, H. Xandri-Monje, J. Zhang, S. H. Ellacott, E. D. H. Mansfield, M. Hartlieb, R. Dallmann, S. Perrier, *Small* **2022**, *18*, 2203070.
- [95] X. Yi, H. Gao, *Nanoscale* **2017**, *9*, 454.
- [96] X. Chen, S. Zhang, J. Li, X. Huang, H. Ye, X. Qiao, Z. Xue, W. Yang, T. Wang, *Adv. Sci.* **2022**, *9*, 2202644.
- [97] A. Bigi, G. Cojazzi, S. Panzavolta, K. Rubini, N. Roveri, *Biomaterials* **2001**, *22*, 763.
- [98] T. J. Merkel, S. W. Jones, K. P. Herlihy, F. R. Kersey, A. R. Shields, M. Napier, J. C. Luft, H. Wu, W. C. Zamboni, A. Z. Wang, J. E. Bear, J. M. DeSimone, *Proc. Natl. Acad. Sci. USA* **2011**, *108*, 586.
- [99] A. Dols-Perez, C. Fornaguera, N. Feiner-Gracia, S. Grijalvo, C. Solans, G. Gomila, *Colloids Surf., B* **2023**, *222*, 113019.
- [100] B. Hoffmann, H. Kosegarten, *Physiol. Plant* **1995**, *95*, 327.
- [101] Y. Mao, M. J. Thompson, Q. Wang, E. W. Tsai, *J. Pharm. Biomed. Anal.* **2004**, *35*, 1127.
- [102] J. L. Hutter, J. Bechhoefer, *Rev. Sci. Instrum.* **1993**, *64*, 1868.
- [103] G. G. Bilodeau, *J. Appl. Mech.* **1992**, *59*, 519.